COMPARISON OF ELECTROMAGNETIC SCATTERING SOLUTIONS USING THE DISK AS A TARGET

Keith D. Trott

Abstract

Results are compared for scattering from a perfectly conducting circular disk using three solutions: A closed form physical optics (PO) solution, a Physical Theory of Diffraction (PTD) solution, and a computer implementation of an exact eigenfunction solution. The far field patterns are compared for various ka values as well and incidence angles for both vertically and horizontally polarized electric fields. For normal incidence, the solutions agree very well. For small ka the agreement is remarkable. As ka increases, the agreement is still good as long as the observation angle θ does not exceed 45°.

The applicability of using the disk as a target to calibrate an RCS measurement range is discussed. The disk calibration curve is a plot of the specular return as a function of bistatic angle. This curve is computed for both horizontal and vertical polarizations and various ka values using the PO and eigenfunction solutions. The specular bistatic RCS (calibration curve) is relatively invariant; hence, the disk is an ideal candidate as a calibration standard for bistatic RCS measurements. Agreement between the PO and eigenfunction solutions for large ka means there is an easy method of generating the applicable calibration curve for a particular disk as long as one remains within the valid angular region for a proper size disk.

1 INTRODUCTION

This report compares three circular disk solutions: A closed form physical optics (PO) solution, the RADC/Syracuse Research Corp. bistatic radar cross-section (BSRCRCS) computer program that utilizes the physical theory of diffraction (PTD), and a computer implementation of an exact eigenfunction solution discussed in references [1] through [4]. These are compared for various ka values as well as incidence angles. The limitations of the PO solution are also discussed. As a by-product of this comparison, the BSRCRCS scattering code solution for the disk is validated against an exact eigenfunction solution. Another issue addressed in this report is the curve, using the disk as a target, used to calibrate an RCS measurement range. The disk calibration curve is a plot of the specular return as a function of bistatic angle. This curve will be computed for both horizontal and vertical polarizations and various ka values using the PO and eigenfunction solutions. The disk has become a possible calibration target for bistatic RCS measurement ranges due to problems encountered using the sphere. The bistatic RCS of a sphere has rapid fluctuations which make it difficult to use as a calibration standard for bistatic radar cross section measurements.

The derivation of the PO solution is given Section 2. The PO solution calculates the scattered field using the geometrical optics (GO) current, where the GO current is denoted by Ufimtsev [5] as the uniform current. He also calculates the field scattered due to the non-uniform current on the edge of the disk. The superposition of fields scattered due to the uniform and non-uniform currents yields the total scattered field. This method is called the PTD. The BSRCRCS scattering code used in our comparison utilizes PTD as its method of solution; however, it is not a closed form solution. The BSRCRCS code is designed for arbitrarily shaped bodies and uses numerical techniques to perform the integrations required to implement the PTD method.

The disk is a coordinate surface in the oblate spheroidal coordinate system [1]; therefore, the exact eigenfunction solution can be found using the degenerate case of the oblate spheroidal functions when they collapse to a disk. Detailed discussions of this approach can be found in [1], [2], [3], and [4]. Mithouard and Hodge [4] provide a computer program and subroutines required to calculate the RCS based on the eigenfunction solution. This com-

puter program was modified by Dominek [6] to allow its use for higher ka values. The program, as modified by Dominek, is used in this analysis. In addition, for grazing incidence of the horizontal polarization, this program was run as a function of ka to determine when the eigenfunction was no longer accurate due to numerical and convergence problems of the computer implementation of the eigenfunction solution. This was done to provide an upper bound on the electrical size of the disk solvable via the eigenfunction computer program. Results for the backscatter case were compared to previously published measured results [1].

The details of the PTD and eigenfunction derivations are not discussed any further in this report. The references provided give detailed analyses of these methods. In the next section, we derive the PO based expression for the bistatic scattered field of a disk illuminated by a plane wave.

2 BISTATIC PHYSICAL OPTICS SOLUTION

A version of this result is given without details in [1], and some of the details can be found in [5]. The following result was derived independently because the results of [1] and [5] have different assumptions and applicable geometry (time convention, plane of incidence, direction of incidence, etc.) than the eigenfunction and BSRCRCS scattering code solutions; therefore, to facilitate the comparisons, it was decided to rederive the result rather than to make the requisite modifications to the previous results. It is included for completeness.

The plane of incidence chosen is the xz plane ($\phi^i = 0$). The geometry for the disk is shown in Figure 1, and the geometry for horizontal and vertical polarization are shown in Figure 2 and Figure 3. For our given plane of incidence, the incident $\mathbf{E}^i$ and $\mathbf{H}^i$ fields are given by

$$\mathbf{E}^{\mathbf{i}}(\mathbf{r}') = \left\{ \begin{array}{c} \hat{\theta}' \\ \hat{\phi}' \end{array} \right\} e^{-j\mathbf{k}^{\mathbf{i}}\cdot\mathbf{r}} \tag{1}$$

where the bracketed term represents the two possible polarizations. The incident magnetic field, $\mathbf{H}^i$, is given by

$$\mathbf{H}^{\mathbf{i}}(\mathbf{r}') = Y_0 \hat{r}^i \times \mathbf{E}^{\mathbf{i}}(\mathbf{r}'). \tag{2}$$

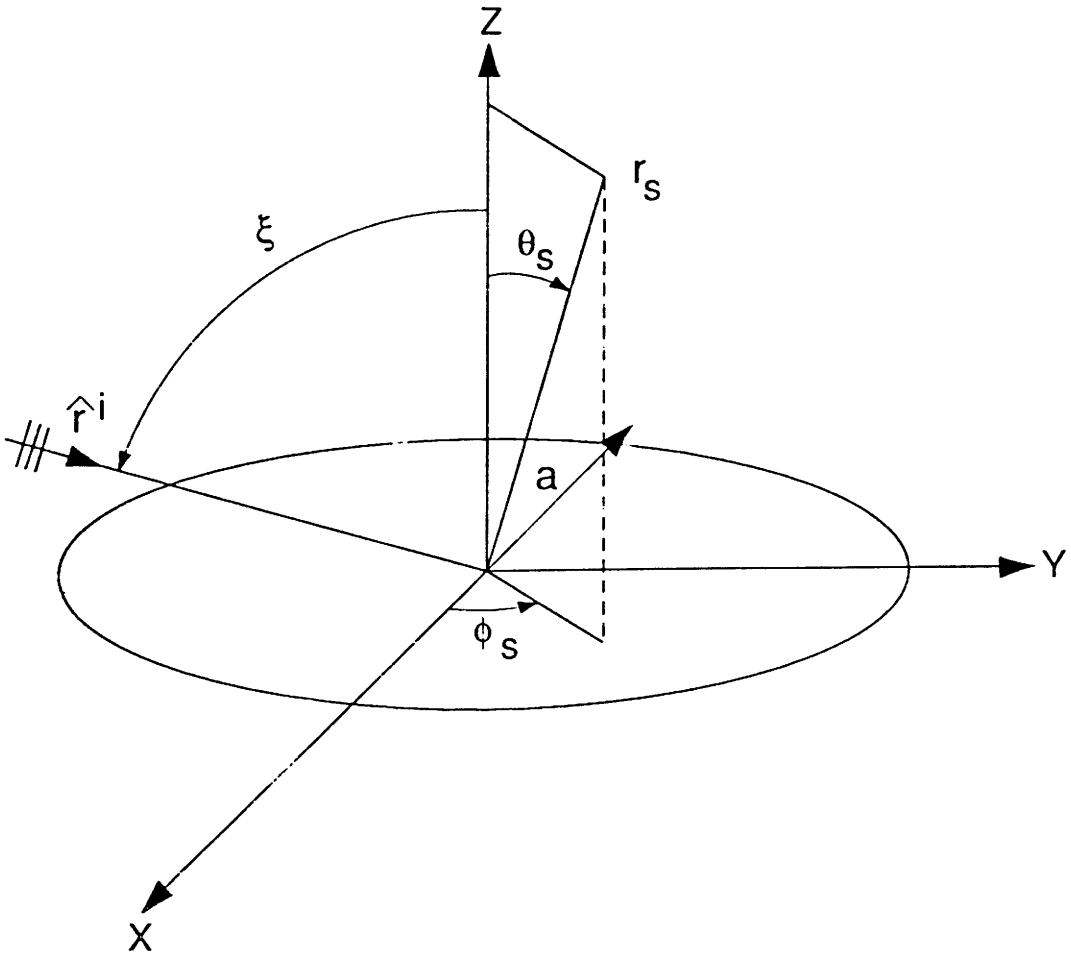

Figure 1: Disk Geometry

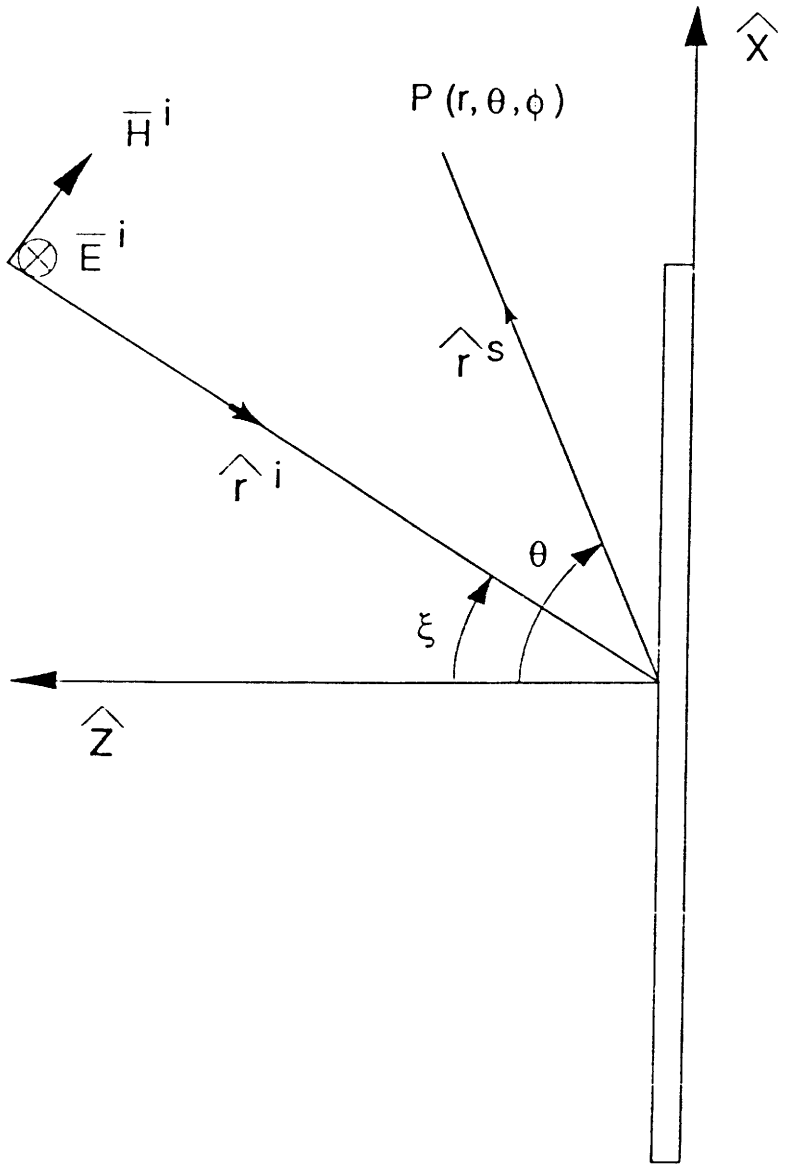

Figure 2: Incident Plane Geometry for Horizontal Polarization (Pol=90)

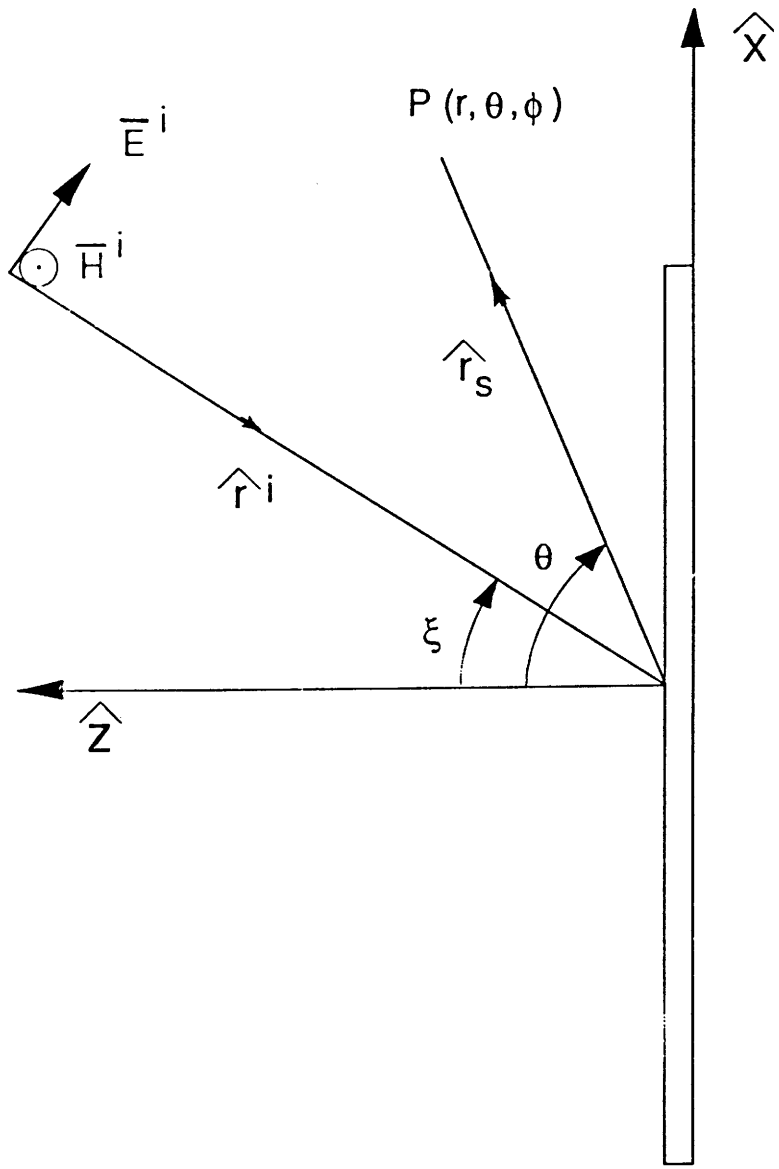

Figure 3: Incident Plane Geometry for Vertical Polarization (Pol=0)

where

$$Y_0 = \sqrt{\frac{\epsilon}{\mu}}, \tag{3}$$

$$k = \frac{2\pi}{\lambda}, \tag{4}$$

$$\hat{r^i} = -\hat{x}\sin\xi - \hat{z}\cos\xi, \tag{5}$$

$$\mathbf{k^i} = k\hat{r^i}, \tag{6}$$

$$\hat{\theta^i} = \hat{x}\cos\xi - \hat{z}\sin\xi, \tag{7}$$

$$\hat{\phi^i} = \hat{y}, \tag{8}$$

and

$$\mathbf{r} = x\hat{x} + y\hat{y} + z\hat{z}. \tag{9}$$

The upper and lower terms in Eq.(1) are for parallel (vertical or theta) and perpendicular (horizontal or phi) polarizations respectively. The polarization of the incident field is parallel/perpendicular with respect to our plane of incidence. In general, the GO current is given by

$$\mathbf{J_{go}}(\mathbf{r'}) = \begin{cases} 2\hat{z} \times \mathbf{H^i}(\mathbf{r'}) & \text{in the lit region, and} \\ 0 & \text{in the shadow region.} \end{cases} \tag{10}$$

hence,

$$\mathbf{J_{go}}(\mathbf{r'}) = 2Y_0 \begin{Bmatrix} \hat{x} \\ \hat{y}\cos\xi \end{Bmatrix} e^{jk\rho'\cos\phi'\sin\xi}. \tag{11}$$

Using this current (making the usual far field approximations) yields an expression for the scattered field given by

$$\mathbf{E^s_{po}}(\mathbf{r}) = jk\frac{e^{-jkr}}{r} \begin{Bmatrix} \hat{r}_i \times \hat{r}_s \times \hat{x} \\ \hat{r}_s \times \hat{r}_s \times \hat{y}\cos\xi \end{Bmatrix} D(\theta, \phi, \xi) \tag{12}$$

where,

$$D(\theta, \phi, \xi) = \frac{1}{2\pi}\int_0^a \rho' \int_0^{2\pi} e^{jk\rho'[\sin\theta\cos(\phi-\phi')+\sin\xi\cos\phi']} d\phi' d\rho'. \tag{13}$$

We can then write the phase term of the integrand in the form

$$\sin\theta\cos(\phi - \phi') + \sin\xi\cos\phi' = \Omega\cos(\gamma - \phi') \tag{14}$$

such that

$$\Omega \cos\gamma = \sin\xi + \sin\theta\cos\phi, \tag{15}$$

$$\Omega \sin\gamma = \sin\theta\sin\phi, \tag{16}$$

$$\Omega = \sqrt{\sin^2\theta\sin^2\phi + (\sin\xi + \sin\theta\cos\phi)^2}. \tag{17}$$

Therefore, we write

$$D(\theta,\phi,\xi) = \int_0^a \rho' \frac{1}{2\pi}\int_0^{2\pi} e^{jk\rho'\Omega\cos(\gamma-\phi')}d\phi' d\rho'; \tag{18}$$

however,

$$\frac{1}{2\pi}\int_0^{2\pi} e^{jk\rho'\Omega\cos(\gamma-\phi')}d\phi' = J_0(k\Omega\rho') \tag{19}$$

where $J_0(\cdot)$ is the Bessel function of order zero. In addition,

$$\int_0^a \rho' J_0(k\Omega\rho')d\rho' = a\frac{J_1(ka\Omega)}{k\Omega}. \tag{20}$$

Hence, the PO scattered field is given by

$$\mathbf{E}^s_{\mathbf{po}}(\mathbf{r}) = ja\frac{e^{-jkr}}{r}\frac{J_1(ka\Omega)}{\Omega}\left\{\begin{array}{c} -\hat{\theta}\cos\theta\cos\phi + \hat{\phi}\sin\phi \\ -\cos\xi\left(\hat{\theta}\cos\theta\sin\phi + \hat{\phi}\cos\phi\right)\end{array}\right\}. \tag{21}$$

We want to identify specific input/output polarization pairs; that is, what is the theta polarized scattered field for a phi polarized incident field. We write this as $E^s_{\theta\phi}$. Therefore, we have the following:

$$E^s_{\theta\theta} = -ja\frac{e^{-jkr}}{r}\frac{J_1(ka\Omega)}{\Omega}\cos\theta\cos\phi, \tag{22}$$

$$E^s_{\phi\theta} = ja\frac{e^{-jkr}}{r}\frac{J_1(ka\Omega)}{\Omega}\sin\phi, \tag{23}$$

$$E^s_{\theta\phi} = -ja\frac{e^{-jkr}}{r}\frac{J_1(ka\Omega)}{\Omega}\cos\xi\cos\theta\sin\phi, \tag{24}$$

$$E^s_{\phi\phi} = -ja\frac{e^{-jkr}}{r}\frac{J_1(ka\Omega)}{\Omega}\cos\xi\cos\phi. \tag{25}$$

Performing appropriate modifications on these expressions yields those given by Ufimtsev [5] for the uniform current.

In general, the scattering cross section is defined by

$$\sigma = \lim_{r\to\infty} 4\pi r^2 \frac{|\mathbf{E}^{\mathrm{s}}|^2}{|\mathbf{E}^{\mathrm{i}}|^2} \tag{26}$$

Additionally, if we desire the polarization dependent cross section, we define

$$\sigma_{ab} = \lim_{r\to\infty} 4\pi r^2 \frac{|\mathbf{E}^{\mathrm{s}}_{\mathbf{a}}|^2}{|\mathbf{E}^{\mathrm{i}}_{\mathbf{b}}|^2} \tag{27}$$

where a and b represent either the theta or phi polarizations. Therefore, the input/output polarization dependent cross section based on Eq.(22) through Eq.(25) is given by

$$\sigma_{\theta\theta} = 4\pi a^2 \left[\frac{J_1(ka\Omega)}{\Omega}\right]^2 \cos^2\theta\cos^2\phi, \tag{28}$$

$$\sigma_{\phi\theta} = 4\pi a^2 \left[\frac{J_1(ka\Omega)}{\Omega}\right]^2 \sin^2\phi, \tag{29}$$

$$\sigma_{\theta\phi} = 4\pi a^2 \left[\frac{J_1(ka\Omega)}{\Omega}\right]^2 \cos^2\xi\cos^2\theta\sin^2\phi, \tag{30}$$

$$\sigma_{\phi\phi} = 4\pi a^2 \left[\frac{J_1(ka\Omega)}{\Omega}\right]^2 \cos^2\xi\cos^2\phi. \tag{31}$$

When the argument of the Bessel function goes to zero we have

$$\lim_{\Omega\to 0} \frac{J_1(ka\Omega)}{\Omega} = \frac{ka}{2} J_0(0) = \frac{ka}{2}. \tag{32}$$

This will be used when evaluating certain limiting cases of the expression.

Two special cases worth discussing are backscatter and specular. In the case of backscatter,

$$\sigma = \pi a^2 \left[J_1(2ka\sin\theta)\right]^2 \cot^2\theta, \tag{33}$$

and for the specular case,

$$\sigma = \frac{4\pi}{\lambda^2}\left(\pi a^2\cos\theta\right)^2. \tag{34}$$

This has the proper form for specular scattering given by

$$\sigma_{spec} = \frac{4\pi}{\lambda^2} A^2 \tag{35}$$

where A is the projected area of the scatterer. Note, both the backscatter and specular expressions are independent of polarization.

These expressions were programmed and used for comparison with both the BSRCRCS scattering code and eigenfunction code. The plots in Section 3 show where the bistatic PO solution for the disk breaks down. In addition, comparisons for the specular response using the PO and eigenfunction solutions will be shown. For our plane of incidence (xz plane), the horizontal polarization has a component parallel to the edge; therefore, for edge-on incidence (incidence angle nearly 90), the scattered field is not zero. The vertical polarization for edge-on incidence, does not have a component parallel to the edge and hence the scattered field is zero. The eigenfunction satifies the proper edge condition; therefore, we expect the proper behavior at the edge. This will be evident in our plots.

3 RESULTS

In this section, plots that compare the three solutions previously described are shown. In addition, calibration curves computed using the PO and eigenfunction solutions are also shown. However, before beginning the comparisons, it is of interest to determine, as a function of electrical circumference of the disk (ka), when the numerical implementation of the eigenfunction solution is valid and when it breaks down. For horizontal polarization, we plotted backscatter and foward scatter for grazing incidence. As expected, the backscatter case accounts for the creeping wave around the disk edge; hence, we see the interference lobes. On the other hand, the forward scatter is not affected by this mechanism and is therefore a smoother curve. Figure 4 shows this behavior. This was accomplished to verify the eigenfunction computer program before using it as a comparison standard. The backscatter case was also compared to published measured results given in [1]. We can see that the numerical implementation of the eigenfunction solution breaks down beyond ka=22 due to numerical convergence problems of the code im-

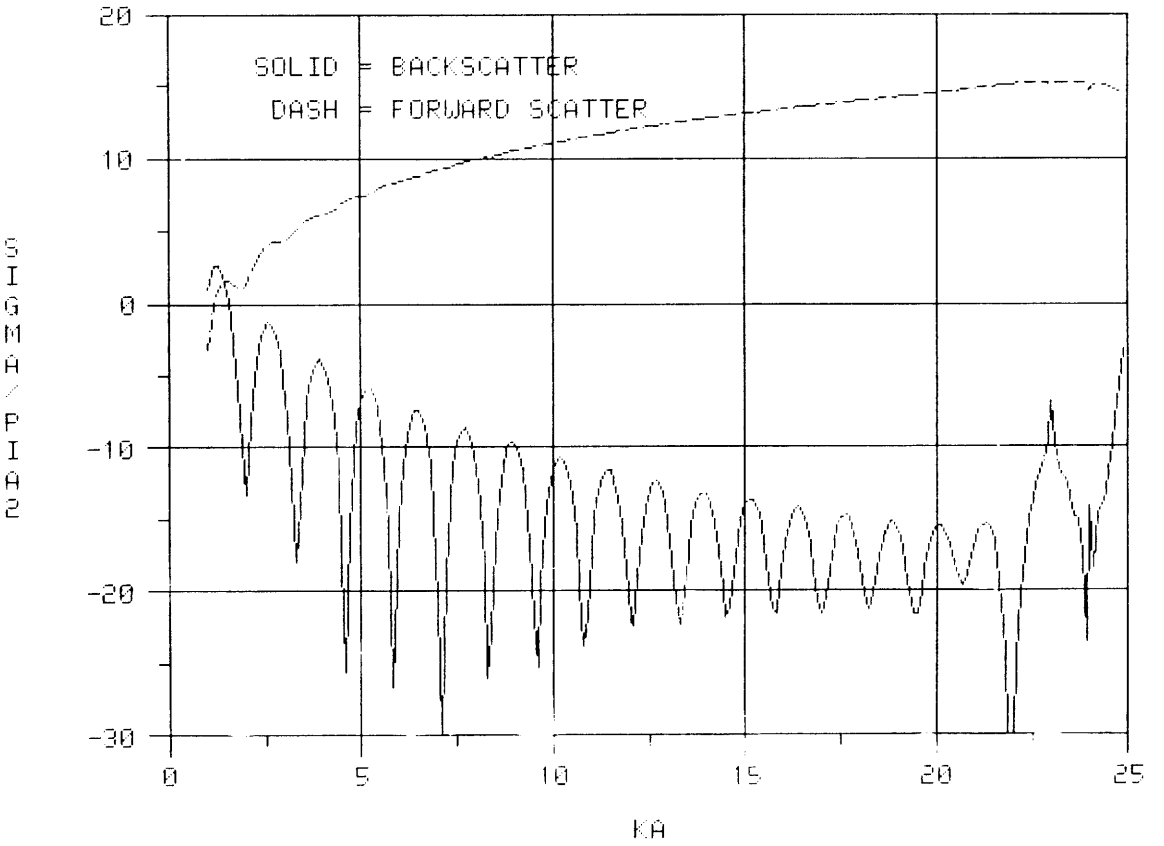

Figure 4: Grazing Incidence ka Plot

plementation. Therefore, we only used the eigenfunction computer code up to ka=20.

Figure 5 through Figure 8 show the bistatic radar cross-section (RCS) of a disk illuminated by a plane wave at normal incidence. The plots shown are for both horizontal and vertical polarization at several ka values. For all these cases the phi observation angle, ϕ^s, equals zero ($\phi^i = \phi^s = 0$). For horizontal polarization (Pol=90), the agreement is better than for vertical polarization (Pol=0). As the disk ka increases and the observation angle θ exceeds 45°, the PO solution begins to break down; however, the agreement between the BSRCRCS code and the eigenfunction code remains reasonable for larger angles, especially for horizontal polarization. The figures included only show this comparison for ka=5 and ka=10; however, the codes were run up to ka=20 and the same trend was observed.

Letting $\phi = 180°$, we are in the quadrant where the specular lies for our given plane of incidence. We see that regardless of how different the results are in general, they agree (within a few dB) at specular ($\theta^i = \theta^s$). Figure 9 through Figure 14 show these results for several incident angles. The agreement at specular gives us hope the calibration curve using the disk

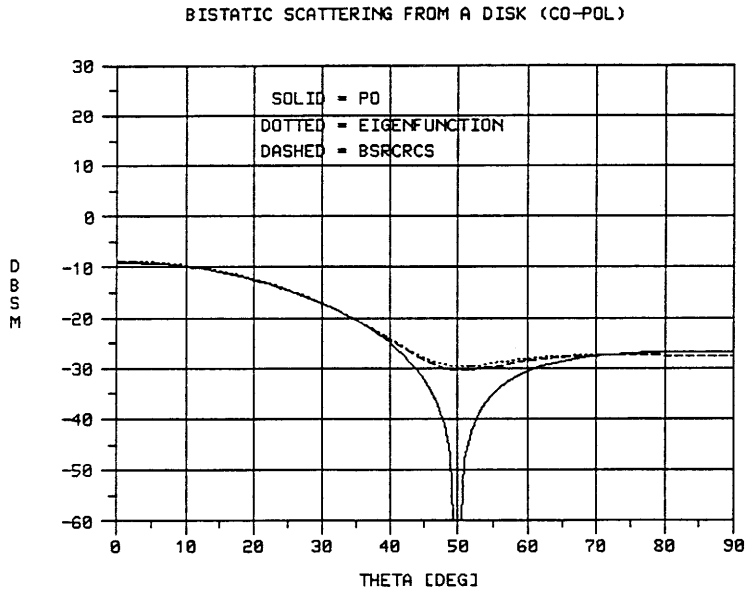

Figure 5: Bistatic Scattering: ka=5: θ^i=0: Horiz Pol: ϕ^i=0: ϕ^s=0

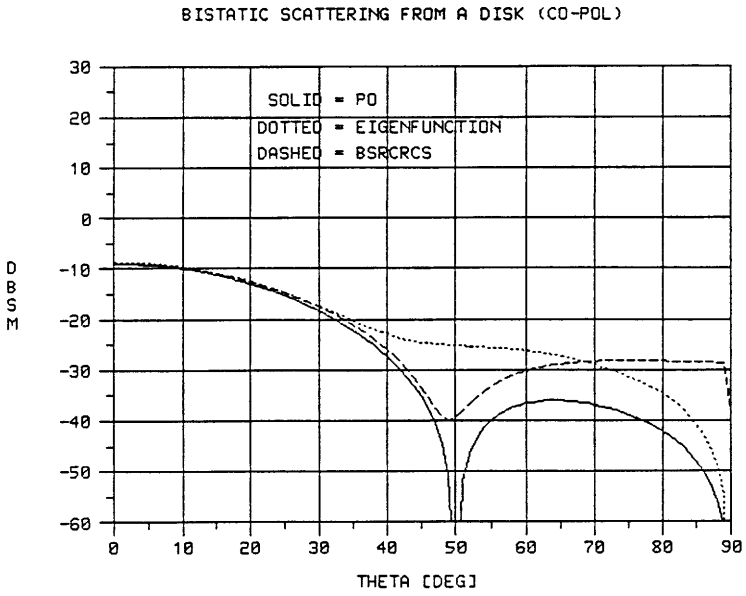

Figure 6: Bistatic Scattering: ka=5: θ^i=0: Vert Pol: ϕ^i=0: ϕ^s=0

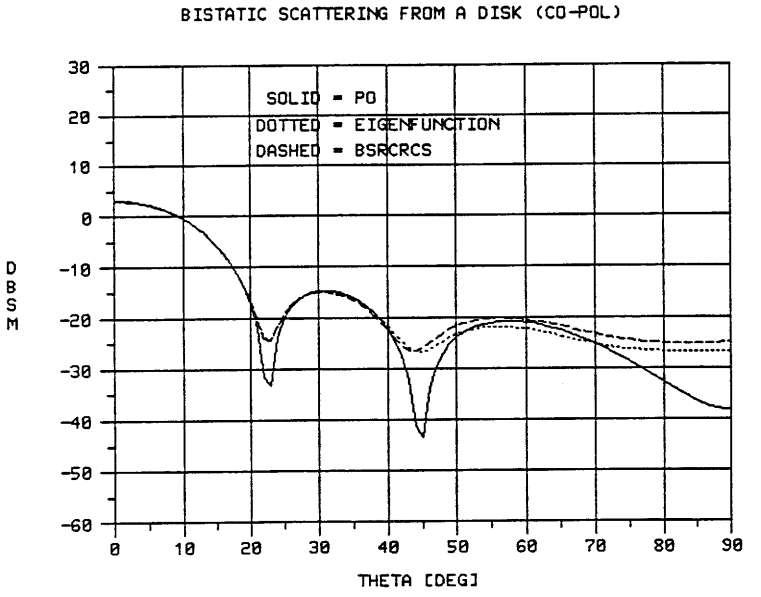

Figure 7: Bistatic Scattering: ka=10: θ^i=0: Horiz Pol: ϕ^i=0: ϕ^s=0

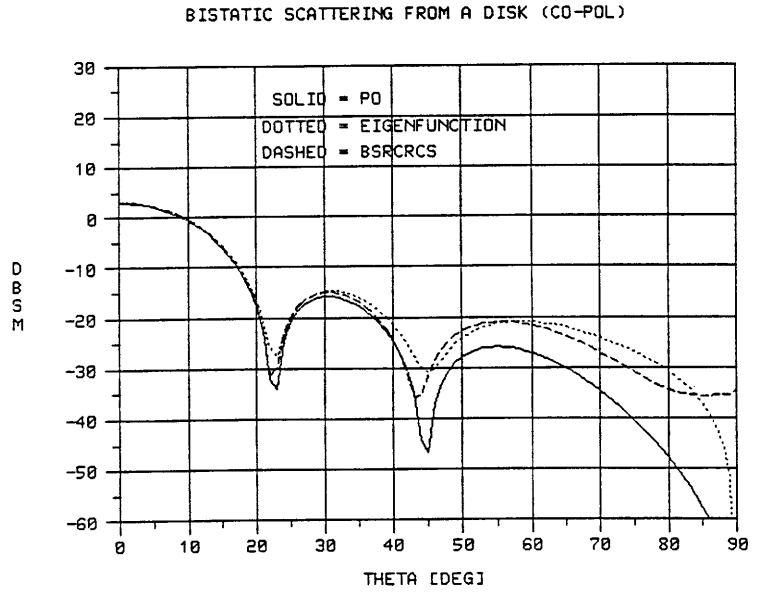

Figure 8: Bistatic Scattering: ka=10: θ^i=0: Vert Pol: ϕ^i=0: ϕ^s=0

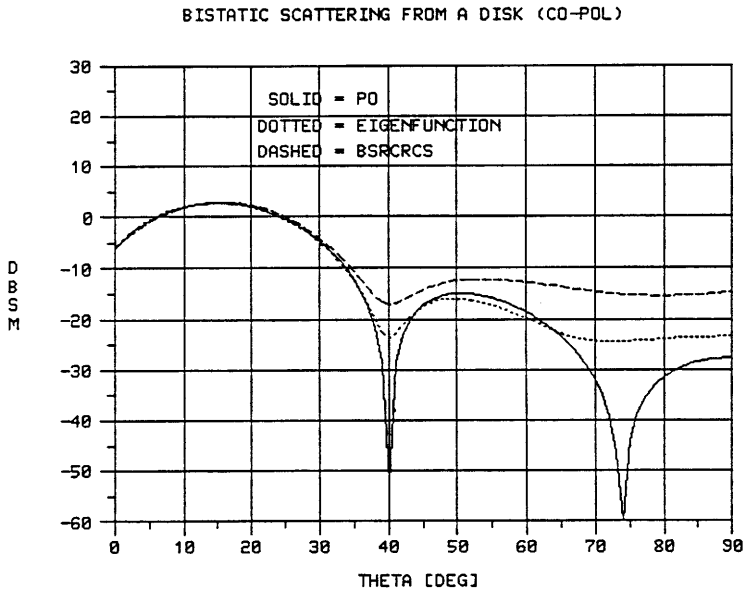

Figure 9: Bistatic Scattering: ka=10: θ^i=15: Horiz Pol: ϕ^i=0: ϕ^s=180

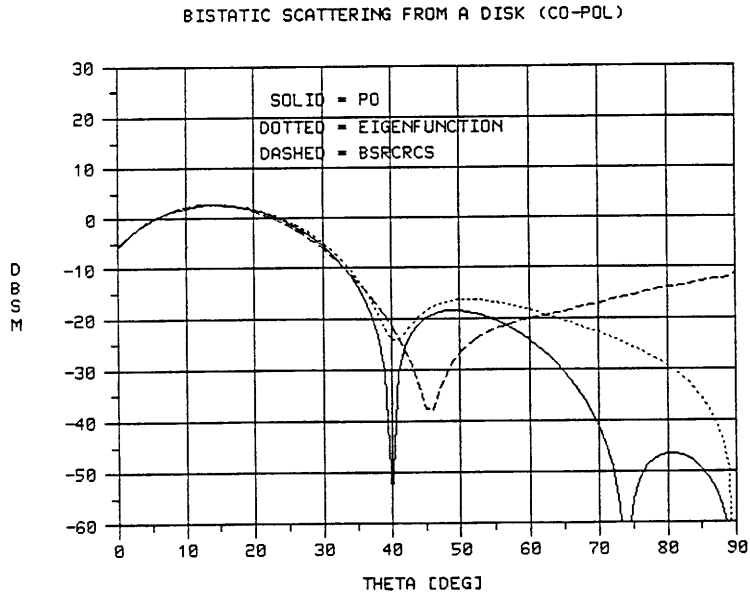

Figure 10: Bistatic Scattering: ka=10: θ^i=15: Vert Pol: ϕ^i=0: ϕ^s=180

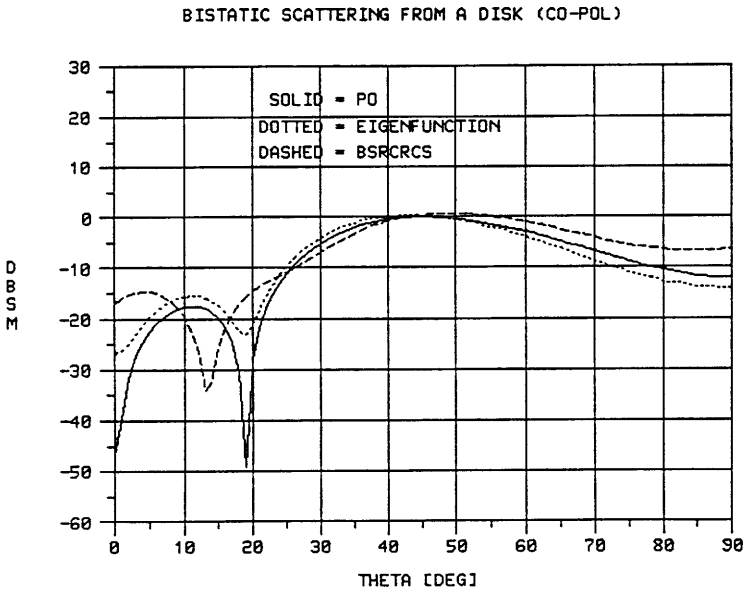

Figure 11: Bistatic Scattering: ka=10: θ^i=45: Horiz Pol: ϕ^i=0: ϕ^s=180

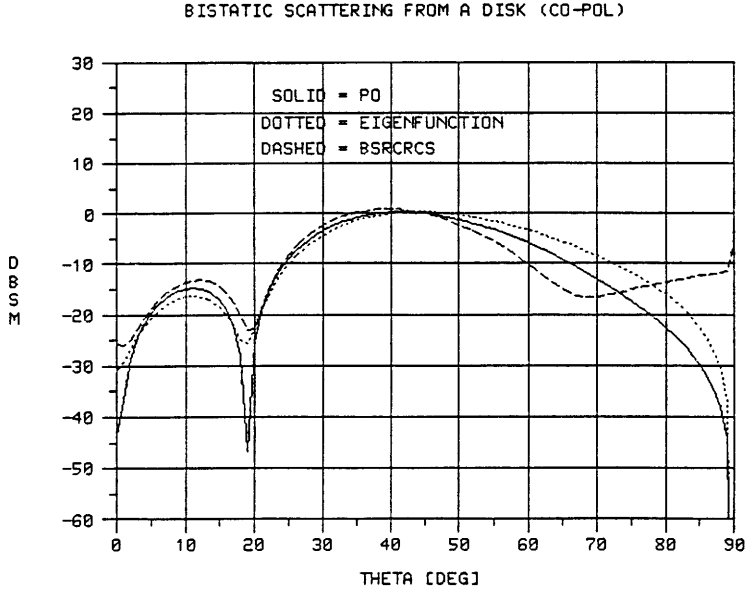

Figure 12: Bistatic Scattering: ka=10: θ^i=45: Vert Pol: ϕ^i=0: ϕ^s=180

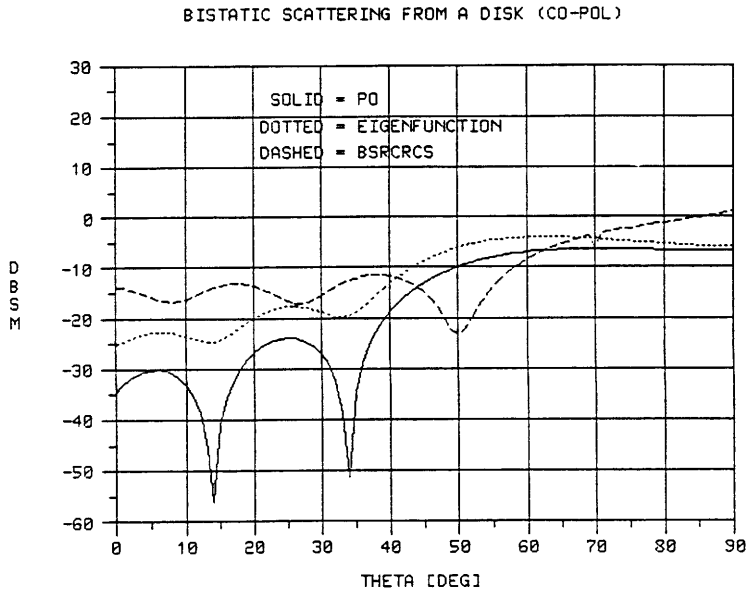

Figure 13: Bistatic Scattering: ka=10: θ^i=70: Horiz Pol: ϕ^i=0: ϕ^s=180

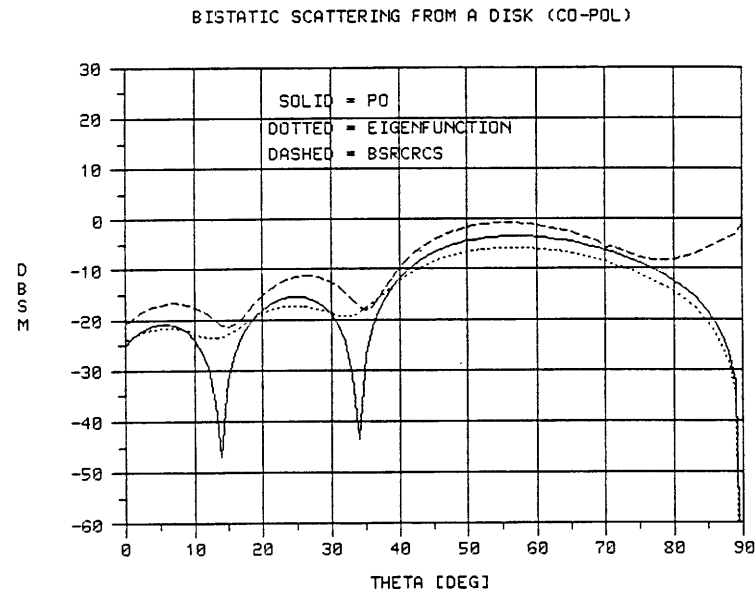

Figure 14: Bistatic Scattering: ka=10: θ^i=70: Vert Pol: ϕ^i=0: ϕ^s=180

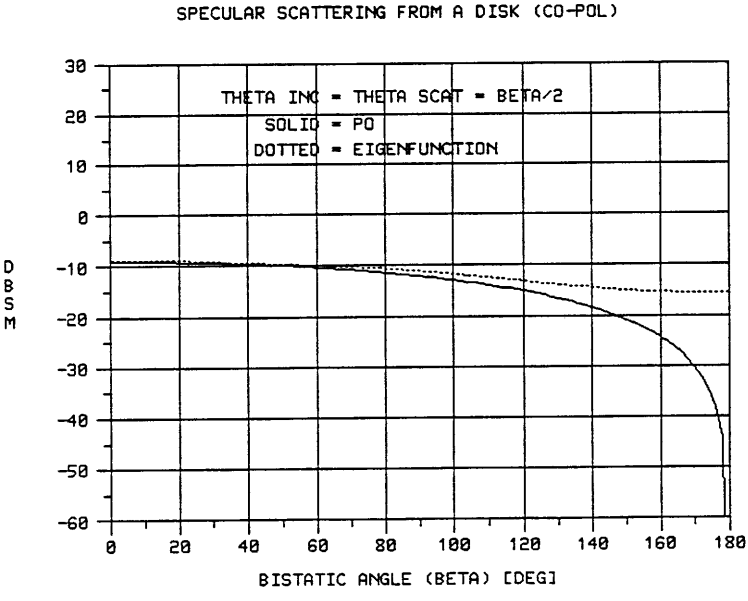

Figure 15: Specular Scattering: ka=5: Horiz Pol

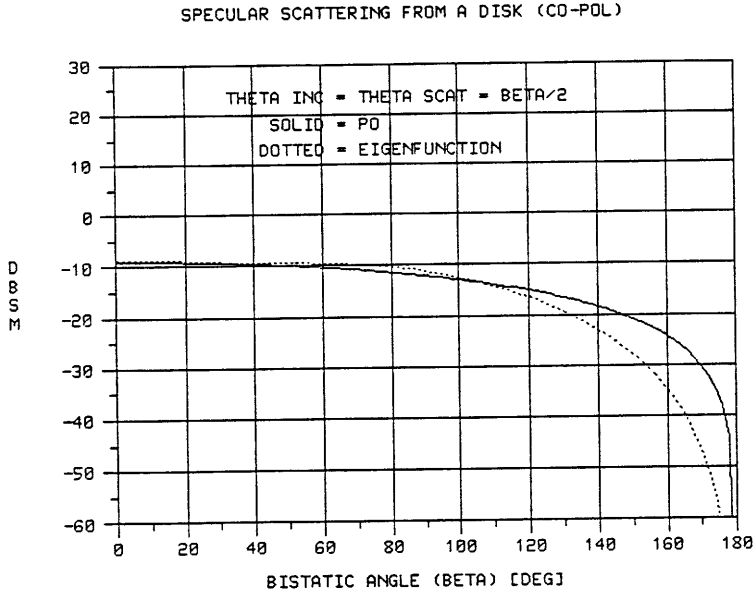

Figure 16: Specular Scattering: ka=5: Vert Pol

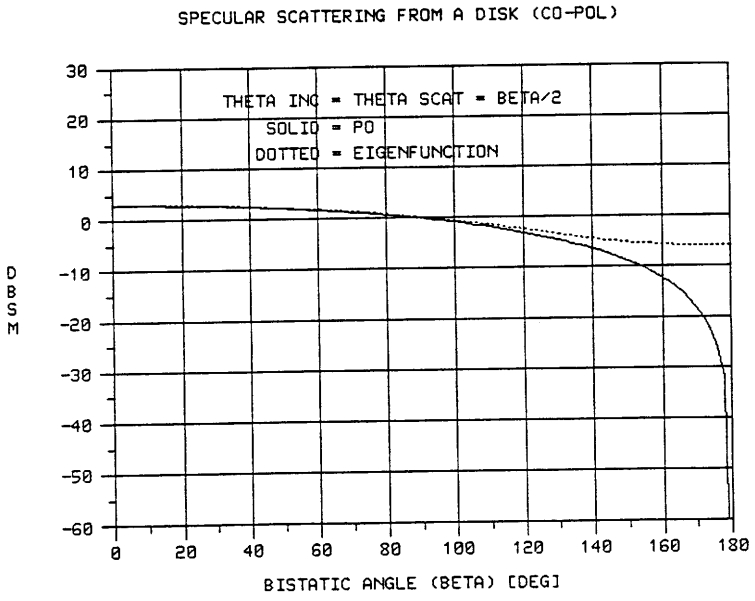

Figure 17: Specular Scattering: ka=10: Horiz Pol

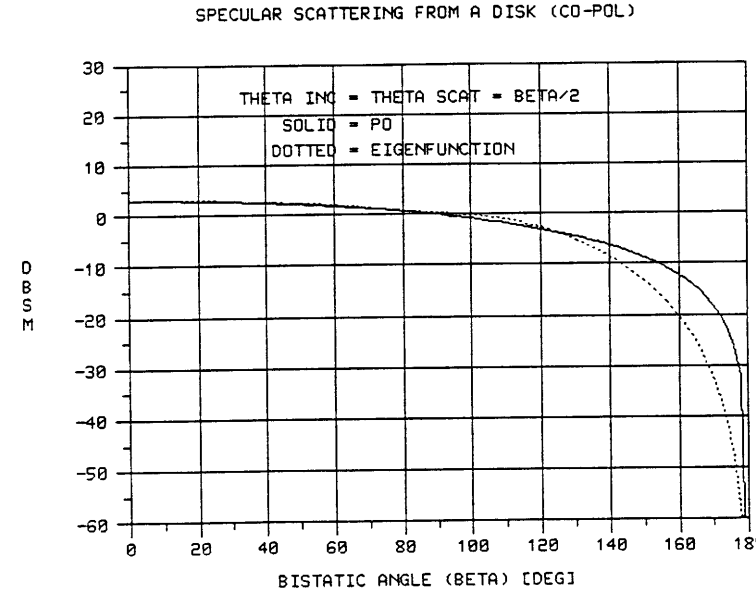

Figure 18: Specular Scattering: ka=10: Vert Pol

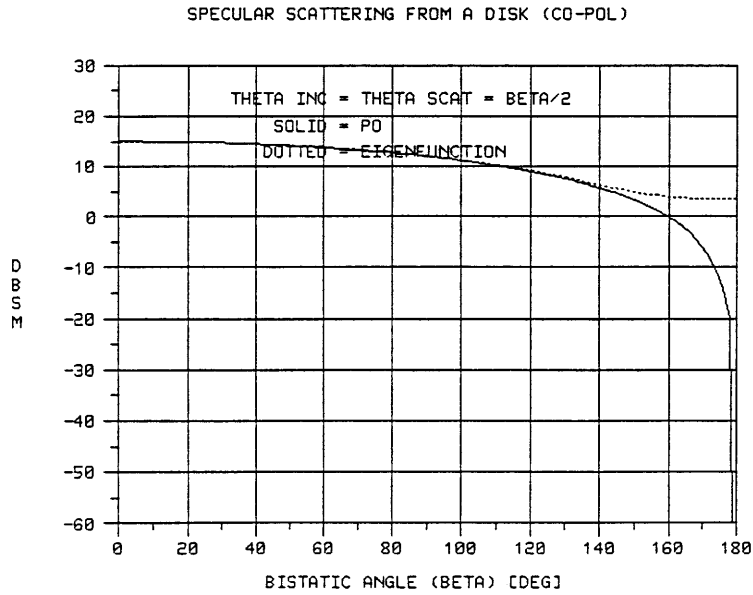

Figure 19: Specular Scattering: ka=20: Horiz Pol

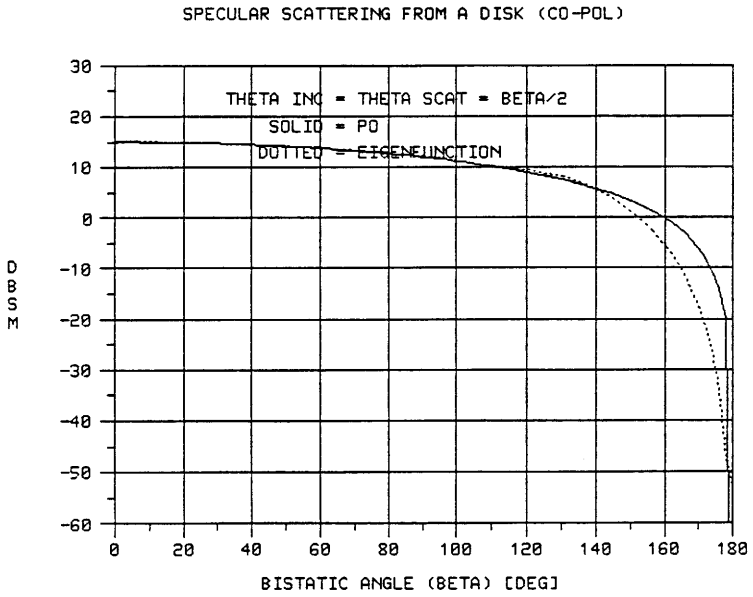

Figure 20: Specular Scattering: ka=20: Vert Pol

as a target will agree over a wide range of bistatic angles. The determination of the calibration curve with a disk target was the primary reason for this analysis.

Plotting the calibration curve, we see that the calibration curve calculated using PO goes to zero for both polarizations; however, the calibration curve calculated using the eigenfunction, as expected, does not. We see reasonable agreement for both polarizations over bistatic angles less than 140°. Figure 15 through Figure 20 show this comparison for several ka values. As ka increases, the agreement between the PO and eigenfunction solutions for specular improves. As we see in Figure 20, for ka = 20 the difference is negligible for $0° < \beta < 140°$.

4 CONCLUSIONS

The numerical implementation of the eigenfunction solution is only useable up to ka=20. This was the determined by observing the behavior of this code as a function of ka. Figure 4 only shows this up to ka=25; however, this code was exercised up to ka=40. In addition, comparison of the backscatter curve from Fig. 4 with published measured results [1] verifies the validity of the this code for lower ka values. Use of this code should be limited to this maximum electrical circumference.

We saw that the PO solution for normal incidence agreed very well over the main lobe and a significant number of side lobes. For small ka the agreement is remarkable. As ka increased, the agreement was still good as long as the observation angle θ did not exceed 45°.

When we concentrate on the specular return from the disk, PO does a good job for incidence angles as large as 70°. This is really not suprising since the specular return is an optics quantity governed by geometrical optics. In fact, the stationary phase evaluation of the PO integral gives, in general, the GO reflected field. As we saw in the calibration curves (specular response), the PO and eigenfunction solutions agree very well for large ka; however, for small ka a correction factor would be needed to use the PO derived curve for calibration.

The bistatic RCS (calibration curve) of the disk is relatively invariant and has no rapid fluctuations. This makes the disk an ideal candidate as a

calibration standard for bistatic RCS measurements. We also saw that the PO and eigenfunction solutions generate equivalent curves over a wide range of bistatic angles ($0° < \beta < 140°$) for large ka. This means there exists an easy method of generating the applicable calibration curve for a particular disk as long as one remains within the valid angular region for a proper size disk.

References

[1] Bowman, J.J., Senior, T.B.A., and Uslenghi, P.L.E. (Editors)(1969) *Electromagnetic and Acoustic Scattering by Simple Shapes*, Chaps 13,14; North Holland Pub. Co., Amsterdam.

[2] Flammer, C. (1953)"The Vector Wave Function Solution of the Diffraction of Electromagnetic Waves by Circular Disks and Apertures, I. Oblate Spheroidal Vector Wave Functions, II. The Diffraction Problem", *J. Appl. Phys.*, Vol 24, No. 9; PP 1218-1231.

[3] Mattson, G.R., (1970) "Electromagnetic Plane Wave Scattering by a Perfectly Conducting Disk", Ph.D. Dissertation, University of Michagan.

[4] Mithouard D.P. and Hodge, D.B.(1979)" Scattering by Metallic Disk", Report 710816-3, The Ohio State University ElectroScience Laboratory, Dept. of Electrical Engineering.

[5] Ufimtsev, P.Ia. (1958)" Approximate Calculation of the Diffraction of a Plane Electromagnetic Wave by Certain Metal Objects, II. The Diffraction by a Disk and by a Finite Cylinder", *Soviet Physics -Technical Physics*, Vol 3, No. 11, pp 2386-2396.

[6] Dominek, A.K., Personal Communication